PERGAMON

Journal of Structural Geology 24 (2002) 517–530

JOURNAL OF STRUCTURAL GEOLOGY

www.elsevier.com/locate/jstrugeo

Lattice- and shape-preferred orientation of orthopyroxene porphyroclasts in peridotites: an application of two-dimensional numerical modeling

Kazuhiko Ishii[a,*], Takashi Sawaguchi[b]

[a]*Division of Science Education, Osaka Kyoiku University, Kashiwara, Osaka 582-8582, Japan*
[b]*Department of Earth Sciences, School of Education, Waseda University, Shinjiku, Tokyo 169-8050, Japan*

Received 14 September 2000; revised 14 May 2001; accepted 15 June 2001

Abstract

Orthopyroxene porphyroclasts in peridotite mylonites are elongated to a variable extent and this variation depends on the crystallographic orientation of grains. We simulated the development of lattice- and shape-preferred orientation of orthopyroxene grains in peridotite using a purely geometrical two-dimensional model. In this model, under the given matrix deformation, orthopyroxene grains are assumed to deform and rotate so as to minimize the difference in displacement between the matrix and grains. In addition, the deformation of an orthopyroxene grain is limited to dislocation glide on the unique slip system (100)[001]. The results show that glide-plane orientation (θ) of grains with a large aspect ratio (R) become separated into two orientations during progressive matrix deformation ranging from simple shear to pure shear. In addition, the degree of asymmetry in $R-\theta$ distribution increases with the degree of non-coaxiality of matrix deformation. In contrast, the long-axis orientation (ϕ) of grains becomes concentrated around the elongation axis of matrix deformation. A natural example from the Horoman peridotite complex, northern Japan, shows an $R-\theta-\phi$ relation consistent with matrix deformation by progressive simple shear. Thus, the $R-\theta-\phi$ relations of orthopyroxene porphyroclasts may be useful for the estimation of strain magnitude as well as the degree of non-coaxiality of deformed peridotites.

Keywords: Lattice-preferred orientation; Shape-preferred orientation; Orthopyroxene porphyroclast; Deformation of peridotite; Numerical model

1. Introduction

Orthopyroxene porphyroclasts in peridotite mylonites are elongated to a variable extent and this variation depends on the crystallographic orientation of grains (Darot and Boudier, 1975; Reuber et al., 1982; Suhr, 1993; Tubía, 1994; Sawaguchi and Takagi, 1997; Sawaguchi et al., 2001). Similar relationships are recognized in orthopyroxene porphyroclasts in granulite facies basic mylonites (Dornbusch et al., 1994; Toyoshima, 1998; Hanmer, 2000). Since (100)[001] is the predominant slip system in orthopyroxene (e.g. Mercier, 1985), a grain favorably oriented for dislocation glide will be highly deformed, while an unfavorably oriented grain will be little deformed during progressive deformation of such mylonites. The following factors affect this relationship between the crystallographic orientation and the grain shape of orthopyroxene:

1. kinematics of deformation in the olivine matrix such as degree of non-coaxiality and strain magnitude;
2. initial shape, long-axis orientation and crystallographic orientation of grains;
3. rheology of grains including critical resolved shear stress of active slip system and rheological contrast between grains and the olivine matrix.

Thus, the lattice- and shape-preferred orientation of orthopyroxene porphyroclasts contains information on kinematics and dynamics of peridotite deformation. In this paper, we present a numerical model for the development of lattice- and shape-preferred orientation of orthopyroxene grains in peridotites and apply the results to a natural example from the Horoman peridotite complex, Hokkaido, Japan.

Various numerical models for the development of lattice-preferred orientation have been proposed and applied to natural and experimental examples. However, the models based on the Taylor (1938) theory, which assumes homogeneous deformation, cannot simulate variable grain deformation depending on their crystallographic orientations (e.g. Lister et al., 1978; Lister and Paterson, 1979; Lister and Hobbs, 1980). This deficiency has been overcome by various methods, such as the purely geometrical models

* Corresponding author. Fax: +81-729-78-3385.
E-mail address: kishii@cc.osaka-kyoiku.ac.jp (K. Ishii).

0191-8141/02/$ - see front matter
PII: S0191-8141(01)00078-5

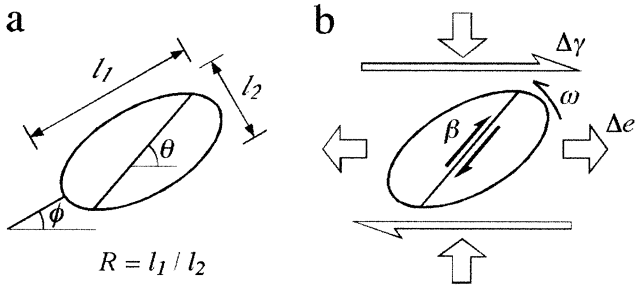

Fig. 1. Parameters used in the simulation. (a) The geometry of a grain. θ; orientation of a glide plane, ϕ; orientation of the long axis of a grain, l_1, l_2; lengths of long and short axes of a grain, R; aspect ratio of a grain. (b) Incremental deformation of the grain and the matrix. Δe, $\Delta\gamma$; pure shear and simple shear components of the incremental matrix deformation, ω; incremental rotation of the grain, β; incremental shear strain of the grain.

(Etchecopar, 1977; Etchecopar and Vasseur, 1987), models using the viscoplastic self-consistent theory (e.g. Molinari et al., 1987; Wenk et al., 1989, 1991; Takeshita et al., 1990) and models using the finite difference method (Zhang et al., 1994; Zhang and Wilson, 1997). In addition, effects of recrystallization on the development of lattice-preferred orientation have also been included in models (e.g. Jessel, 1988a,b; Jessel and Lister, 1990; Wenk and Tomé, 1999). These previous models have simulated the development of lattice-preferred orientation of mono-mineralic (e.g. quartzite or dunite) or two-phase (e.g. olivine–orthopyroxene mixture) mineral aggregates. In contrast, the present model simulates large grains embedded in a fine-grained matrix (i.e. orthopyroxene porphyroclasts in a fine-grained olivine matrix). In addition, the present model is able to trace not only the change in crystallographic orientation but also the change in grain shape of orthopyroxene. Grains with a different shape are shown to behave differently, even if their crystallographic orientations are identical. The models that allow inhomogeneous deformation show that favorably oriented grains for dislocation glide are highly deformed and unfavorably oriented grains are little deformed (e.g. Etchecopar, 1977; Wenk et al., 1991; Zhang et al., 1994). However, detailed relations between grain shape and their crystallographic orientation have not been analyzed in previous numerical models.

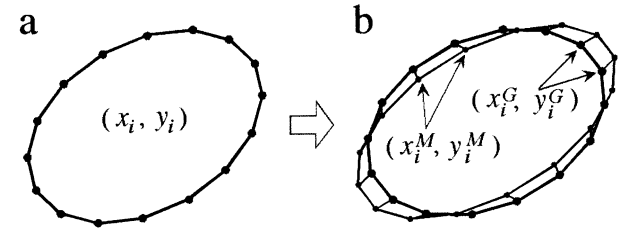

Fig. 2. An incremental deformation step in the simulation method. (a) The outline of the grain before a deformation increment is defined by points (x_i, y_i). (b) (x_i^M, y_i^M) are the positions of (x_i, y_i) after a deformation increment assuming no ductility contrast between the grain and matrix. The positions for the grain (x_i^G, y_i^G) after a deformation increment is determined so as to minimize expression (3).

2. Simulation model

We present here a purely geometrical, two-dimensional numerical model in which deformation of orthopyroxene grains in peridotites are simulated. We consider an elliptical grain with single glide plane within a matrix (Fig. 1a). Thus, a grain can be characterized by its long-axis orientation (ϕ), aspect ratio (R) and the orientation of the glide plane (θ). The matrix is assumed to be deformed by a combination of pure shear (e) and simple shear (γ), where the shear-plane orientation of the simple shear component is parallel to the elongation-axis orientation of the pure shear component. The shear sense of the simple shear component is dextral (Fig. 1b). The relative magnitude of these components is constant during progressive deformation. In response to matrix deformation, the grains deform by superposition of rigid body rotation (ω) and simple shear parallel to the glide plane (β). Thus we need to determine the magnitudes of β and ω during an incremental matrix deformation (Δe and $\Delta\gamma$).

First, the outline of a grain is defined by regularly spaced points (x_i, y_i) (Fig. 2a). Next, we consider the displaced positions of these points (x_i^M, y_i^M) after a deformation increment. Assuming the grain has the same ductility as the matrix, they are written as:

$$\begin{pmatrix} x_i^M \\ y_i^M \end{pmatrix} = \begin{pmatrix} 1+\Delta e & \Delta\gamma \\ 0 & 1-\Delta e \end{pmatrix} \begin{pmatrix} x_i \\ y_i \end{pmatrix} \tag{1}$$

Since the grain deformation is constrained to rotation and simple shear parallel to the glide plane, the grain new positions (x_i^G, y_i^G) should be represented by:

$$\begin{pmatrix} x_i^G \\ y_i^G \end{pmatrix} = \begin{pmatrix} \cos\omega & -\sin\omega \\ \sin\omega & \cos\omega \end{pmatrix} \begin{pmatrix} \cos\theta & -\sin\theta \\ \sin\theta & \cos\theta \end{pmatrix} \begin{pmatrix} 1 & \beta \\ 0 & 1 \end{pmatrix} \times \begin{pmatrix} \cos\theta & \sin\theta \\ -\sin\theta & \cos\theta \end{pmatrix} \begin{pmatrix} x_i \\ y_i \end{pmatrix} \tag{2}$$

The rotation (ω) and shear strain (β) of the grain are determined so as to minimize the following expression:

$$\sum_i \sqrt{(x_i^G - x_i^M)^2 + (y_i^G - y_i^M)^2} \tag{3}$$

New grain positions (Eq. (2)) and new glide-plane orientation ($\theta + \omega$) are determined from this ω and β; then, the next deformation increment is computed. In natural deformation, 'the difference in displacement between the grain and its matrix' is considered to be accommodated by inhomogeneous matrix flow around the grain. We can consider the minimization of expression (3) to imply the minimization of this inhomogeneity. Since fine-grained olivine aggregates are expected to be less anisotropic than an orthopyroxene grain, due to multiple slip systems activated in plastic flow (e.g. Mercier, 1985; Takeshita et al., 1990), their deformation may be geometrically less constrained.

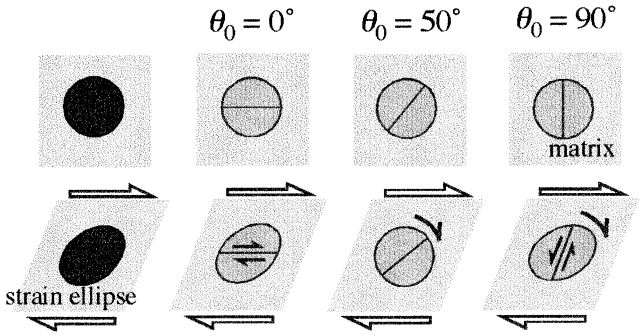

Fig. 3. Deformations and rotations of model circular grains with different glide-plane orientations (θ_0) in a matrix deforming by simple shear.

Therefore, this accommodation is considered to be plausible. The principle of 'minimum difference in displacement' is used in Etchecopar's (1977) model for the development of lattice preferred orientation of polycrystalline aggregates with a single slip system. The same principle has also been used in a model for the development of pressure fringes around rigid grains in a flowing matrix (Etchecopar and Malavieille, 1987; Ishii, 1995).

We computed progressive deformation of initially circular grains with variable glide-plane orientations for three cases of matrix deformation, $\Delta\gamma/\Delta e = \infty$, 2 and 0.

3. Simulation results

3.1. Typical behavior of model grains

Fig. 3 shows behavior of three grains with different initial orientations of the glide plane (θ_0) within a simple shearing matrix ($\Delta\gamma/\Delta e = \infty$). The grain with $\theta_0 = 0°$ is deformed only by simple shear without any additional rigid body rotation ($\omega = 0$). In this case, grain deformation is identical to matrix deformation because the glide plane of the grain is parallel to the shear plane of matrix deformation. Alternatively, the grain with $\theta_0 = 90°$ is deformed with a shear sense opposite to matrix deformation (antithetic shear) with an additional clockwise rigid body rotation. The grain with $\theta_0 = 50°$ rotates clockwise with little deformation.

It is clear that the change in R represents shear deformation of the grain (β), while the change in θ represents the rotation of the grain (ω). On the other hand, the long-axis orientation (ϕ) is changed by both the rotation and the deformation of the grain.

Fig. 4 shows progressive deformation of a grain with $\theta_0 = 90°$ in a matrix deforming by progressive simple shear ($\Delta e = 0$, $\Delta\gamma = 0.02$) up to 360 deformation increments (n). Until $n \approx 80$, the grain is deformed with the shear sense opposite to matrix deformation, and the grain elongates gradually. A concurrent clockwise rotation of the glide plane results in a change in shear sense of the grain deformation. The aspect ratio (R) of the grain therefore

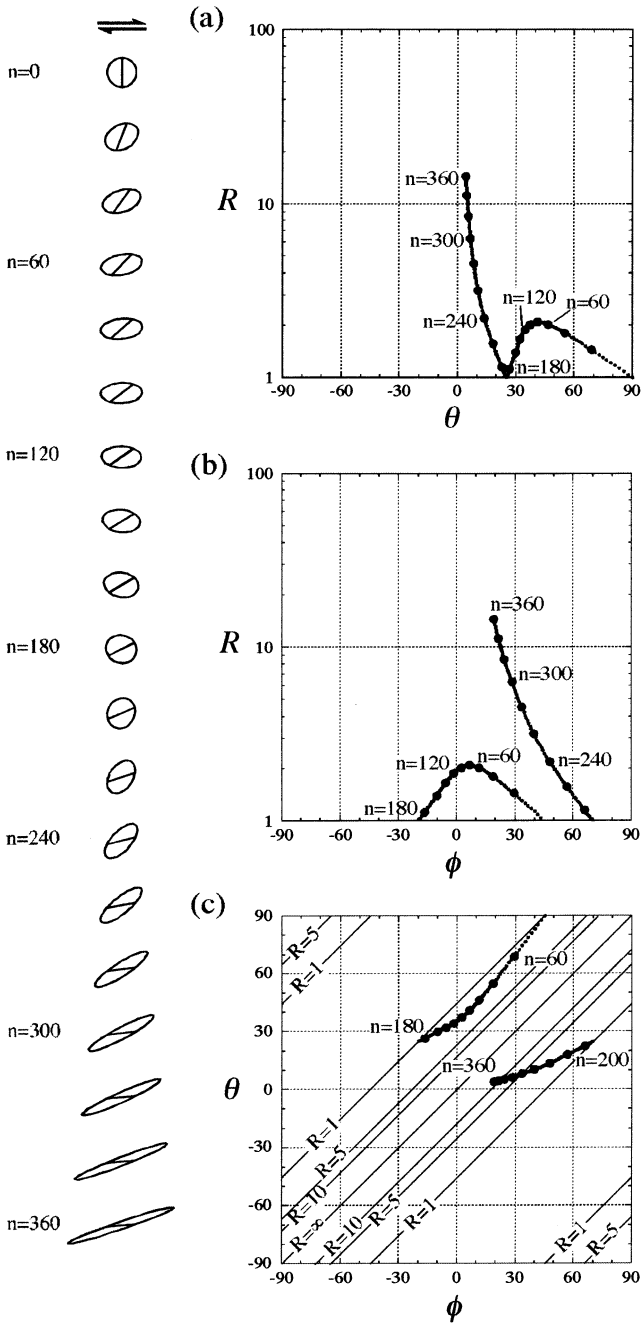

Fig. 4. A progressive deformation of a grain with $\theta_0 = 90°$ in a matrix deforming by progressive simple shear ($\Delta e = 0$, $\Delta\gamma = 0.02$). n is the number of deformation increments. The deformation path of this grain is shown in R–θ (a), R–ϕ (b) and θ–ϕ (c) graphs. See Fig. 1 for these parameters.

decreases after $n \approx 80$. After this stage, the grain continues to deform with the same shear sense as its matrix (synthetic shear). Thus, the grain elongates again after unstraining to a circular shape ($R = 1$) at $n \approx 190$. Note that the change in R from increase to decrease corresponds to the change in shear sense of grain deformation. The long-axis orientation (ϕ) continues to rotate clockwise, except for jumping by 90° when the grain is unstrained to the circular shape (e.g. at

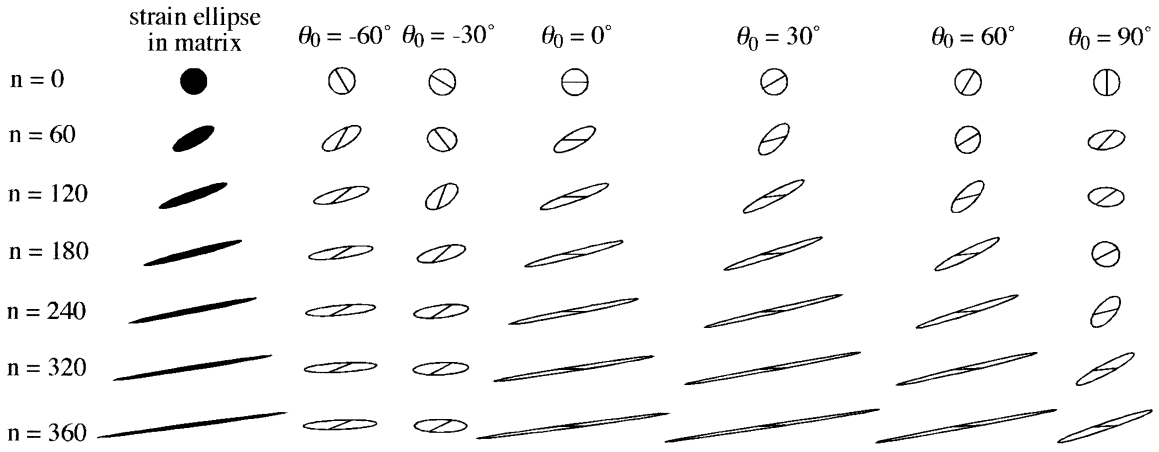

Fig. 5. Progressive deformation of grains with variable θ_0 in a matrix deforming by progressive simple shear ($\Delta e = 0$, $\Delta\gamma = 0.02$).

$n \approx 190$). At this jump in ϕ value, the relative orientation between θ and ϕ changes from $\theta > \phi$ to $\theta < \phi$. Since the grain is deformed by progressive simple shear parallel to the glide plane, the angle between the long axis and the glide plane of the grain ($|\theta - \phi|$) is 45° at the beginning of the deformation. This angle decreases with increasing R (R contours in Fig. 4c).

3.2. Progressive simple shear

Figs. 5 and 6 show progressive deformation of several grains with different θ_0 in a matrix deforming by progressive simple shear ($\Delta e = 0$, $\Delta\gamma = 0.02$). Grains with $-20° \leq \theta_0 \leq 30°$ deform with the same shear sense as the matrix deformation and their R increases monotonously. Among them, grains with $0° < \theta_0 \leq 30°$ rotate clockwise toward the orientation of $\theta = 0°$. Grains with $-20° \leq \theta_0 < 0°$ rotate clockwise during an early stage of the deformation, then rotate counter-clockwise toward the orientation of $\theta = 0°$ during a later stage of the deformation. A small rotation rate of these grains can be ascribed to their glide-plane orientation sub-parallel to the shear plane of the matrix deformation. Grains with $\theta_0 \leq -30°$ and $\theta_0 \geqq 30°$ rotate clockwise more quickly during an early stage of the deformation. In addition, the shear sense of grain deformation changes during progressive deformation. The behavior of a grain with $\theta_0 = 60°$ is similar to that of a grain with $\theta_0 = 90°$, which includes initial antithetic and later synthetic shear and unstraining to the circular shape ($R = 1$). On the contrary, a grain with $\theta_0 = -30°$ experiences the change in shear sense of the grain deformation twice, from synthetic to antithetic and antithetic to synthetic. This change in shear sense of grain deformation is shown by R maxima (Fig. 6). Grains with $-90° < \theta_0 \leq -30°$ show very small rotation and deformation rates during the interval defined by $\theta = 20 \sim 40°$, $\phi = 0 \sim 20°$ and $R > 2$. Typical examples are grains with $-60° \leq \theta_0 \leq -30°$ at $n = 240 \sim 360$ as shown in Fig. 5. Like grains with $60° \leq \theta_0 \leq 90°$, grains with $-60° \leq \theta_0 \leq -30°$ are unstrained to a circular shape ($R = 1$ at $\theta \approx 20°$) and rotate toward the orientation of $\theta = 0°$ after a very large amount of matrix deformation ($n > 1000$). The long-axis orientation (ϕ) of all grains rotate

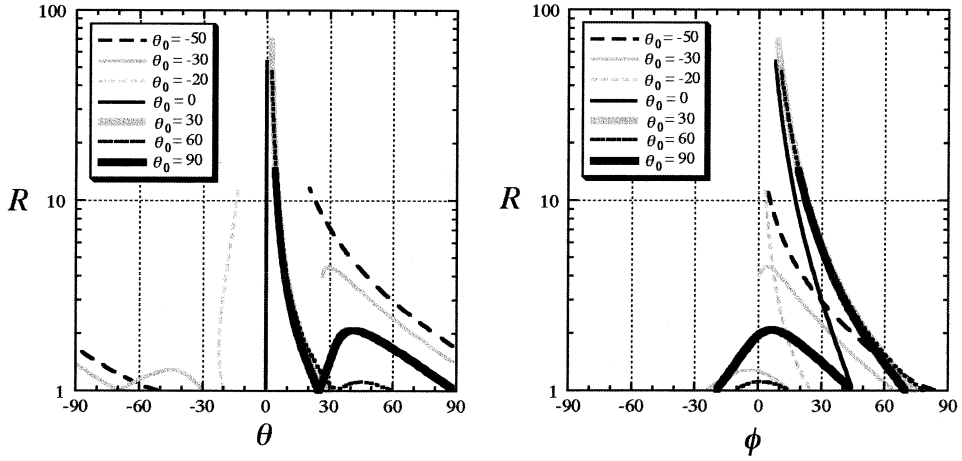

Fig. 6. Progressive change in R, θ and ϕ of grains with variable θ_0 in a matrix deforming by progressive simple shear ($\Delta e = 0$, $\Delta\gamma = 0.02$) to $n = 360$. Note that grains with $\theta_0 = -30°$ and $-50°$ unstrained to circular shape ($R = 1$), as a grain with $\theta_0 = 90°$, after a very large amount of matrix deformation.

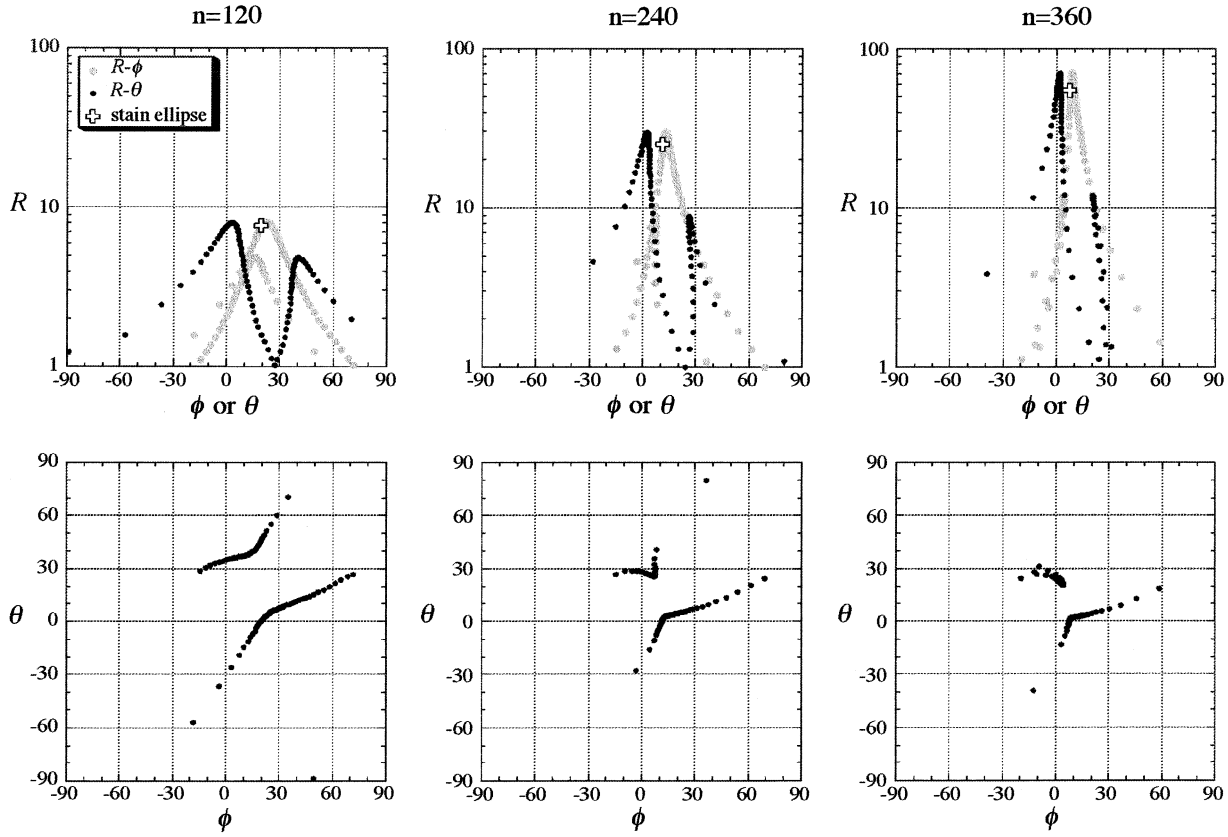

Fig. 7. Progressive development of lattice- and shape-preferred orientation of grains in a matrix deforming by progressive simple shear ($\Delta e = 0$, $\Delta\gamma = 0.02$).

clockwise, except for jumping by 90° when the grains are unstrained to the circular shape.

Fig. 7 shows $R-\theta$, $R-\phi$ and $\theta-\phi$ relations of 90 grains with variable θ_0 (2° intervals) at three different stages of matrix deformation. With increasing matrix deformation, these grains are separated into two groups: one with $\theta < \phi$ and another with $\theta > \phi$. θ distribution of grains with $\theta < \phi$ become concentrated around the shear-plane orientation of matrix deformation ($\theta = 0°$). In contrast, θ distribution of grains with $\theta > \phi$ become concentrated around $20 \sim 40°$, rotating clockwise slowly with matrix deformation. ϕ of the first group are concentrated around $\phi = 10 \sim 30°$, and that of the second group around $\phi = 0 \sim 20°$, overlapping each other. Overall, ϕ distribution are sub-parallel to the elongation axis of matrix deformation. Maximum R of the first group is larger than that of the second group. Geometry of the grain with maximum R can be correlated with deformation geometry of the matrix. Their θ and ϕ imply sub-parallelism to the shear plane and the elongation axis of matrix deformation, respectively, and their R is slightly larger than the axial ratio of the finite strain ellipse for matrix deformation.

Figs. 4 and 7 show that the grain with $\theta_0 = 90°$ belongs to the second group during an early deformation stage ($n = 60 \sim 120$), but belongs to the first group during a later stage ($n \geqq 240$). The second group disappears after a very large amount of matrix deformation, because grains in this group are transferred to the first group after unstraining to circular shape. It should be pointed out that the orientation of $\theta = 0°$ is rotationally stable and all grains rotate toward this orientation. In contrast, grains with large R in the second group rotate very slowly but are not in stable orientation.

3.3. Progressive pure shear

Figs. 8 and 9 show progressive deformation of several grains with different θ_0 in a matrix deforming by progressive pure shear ($\Delta e = 0.01$, $\Delta\gamma = 0$). Grains with $\theta_0 = 0°$ and $\theta_0 = 90°$ do not rotate and are not deformed. Grains with $0° < \theta_0 < 90°$ continue to deform with sinistral shear sense, thus their R increases monotonously. While grains with $30° \leq \theta_0 < 90°$ rotate clockwise, grains with $0° < \theta_0 \leq 20°$ change the rotational sense as deformation proceeds, from clockwise through counter-clockwise, and again to clockwise. θ of all these grains approaches 0° finally. The long-axis orientation (ϕ) of all these grains approaches 0° during a later deformation stage, but changes in ϕ during an early deformation stage are variable depending on their θ_0. The behavior of the grains with $-90° < \theta_0 < 90°$ is a mirror image of that of grains with $90° > \theta_0 > 0°$. Therefore, $R-\phi$ and $R-\theta$ graphs are symmetrical with respect to $\phi = 0°$ and $\theta = 0°$. Hence only grains with $\theta_0 \geqq 0°$ are shown in these figures.

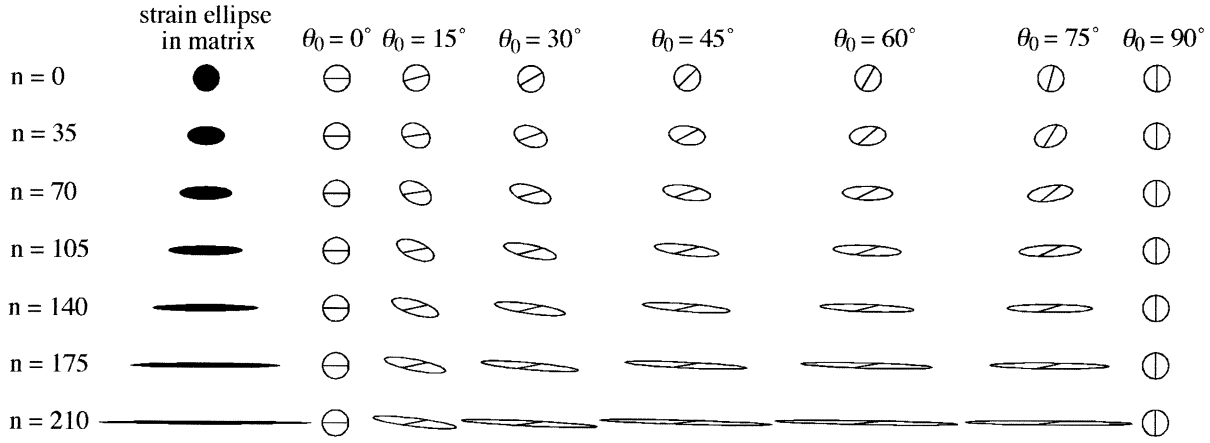

Fig. 8. Progressive deformation of grains with variable θ_0 in a matrix deforming by progressive pure shear ($\Delta e = 0.01$, $\Delta\gamma = 0$).

Fig. 10 shows $R-\theta$, $R-\phi$ and $\theta-\phi$ relations of 90 grains with variable θ_0 (2° intervals) at three different stages of matrix deformation. Grains are separated into two groups as in the case of progressive simple shear. However, in progressive pure shear, two groups are symmetrical with respect to the elongation axis of matrix deformation (i.e. $\phi = 0°$ and $\theta = 0°$). In addition, maximum Rs in two groups are equal and slightly smaller than the axial ratio of the finite strain ellipse for matrix deformation. ϕs of grains with maximum R in both groups are sub-parallel to the elongation axis of matrix deformation. θs of grains with maximum R in both groups approach 0° and two groups merge after a very large amount of matrix deformation.

3.4. Progressive general shear

Figs. 11 and 12 show progressive deformation of several grains with different θ_0 in matrix deforming by progressive general shear ($\Delta e = 0.005$, $\Delta\gamma = 0.01$). Grains with $-50° \leq \theta_0 \leq 20°$ rotate clockwise or counter-clockwise toward the orientation of $\theta \approx -5°$ and their R increases monotonously. Grains with $-90° \leq \theta_0 \leq -60°$ and $30° \leq \theta_0 \leq 90°$ rotate clockwise. Grains with $60° \leq \theta_0 \leq 90°$ increase their R monotonously. This behavior is the same as that of progressive pure shear. However, grains with $30° \leq \theta_0 \leq 59°$ experience unstraining to circular shape, then rotate toward $\theta \approx -5°$ and their R increases monotonously. This behavior is similar to that of progressive simple shear. $\theta_0 = 60°$ is approximately the boundary between these two different types of behavior. This grain shows almost no deformation and rotation during a later deformation stage ($n \geqq 120$) as shown in Fig. 11.

Fig. 13 shows $R-\theta$, $R-\phi$ and $\theta-\phi$ relations of 90 grains with variable θ_0 (2° intervals) at three different stages of matrix deformation. Grains are separated into two groups with different maximum R. However, the difference in maximum R in both groups is smaller than that for the matrix deformation of progressive simple shear. As in cases of progressive simple and pure shear, these two groups are separated by a line with $\theta = \phi$ in a $\theta-\phi$ graph. Grains with maximum R shows almost the same shape and orientation (R and ϕ) as those of the finite strain ellipse for matrix deformation. Two groups merge after a very large amount of matrix deformation, as in the case of progressive pure shear.

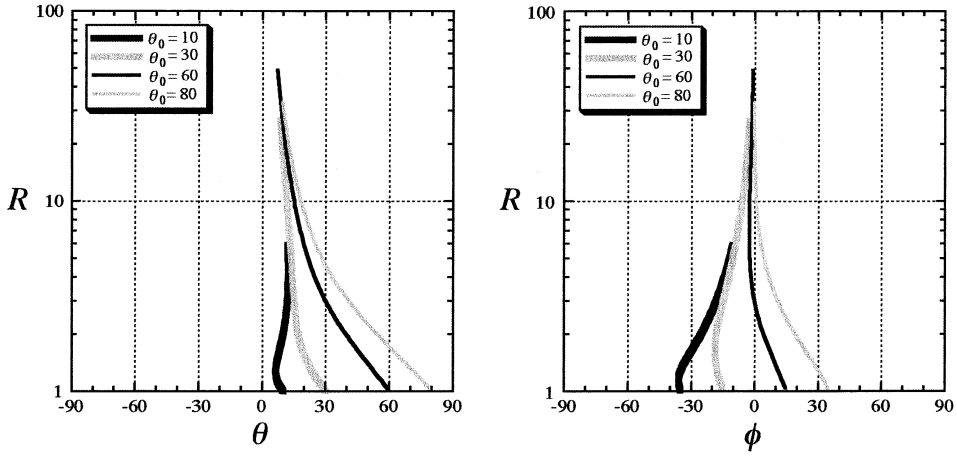

Fig. 9. Progressive change in R, θ and ϕ of grains with variable θ_0 in a matrix deforming by progressive pure shear ($\Delta e = 0.01$, $\Delta\gamma = 0$) to $n = 210$.

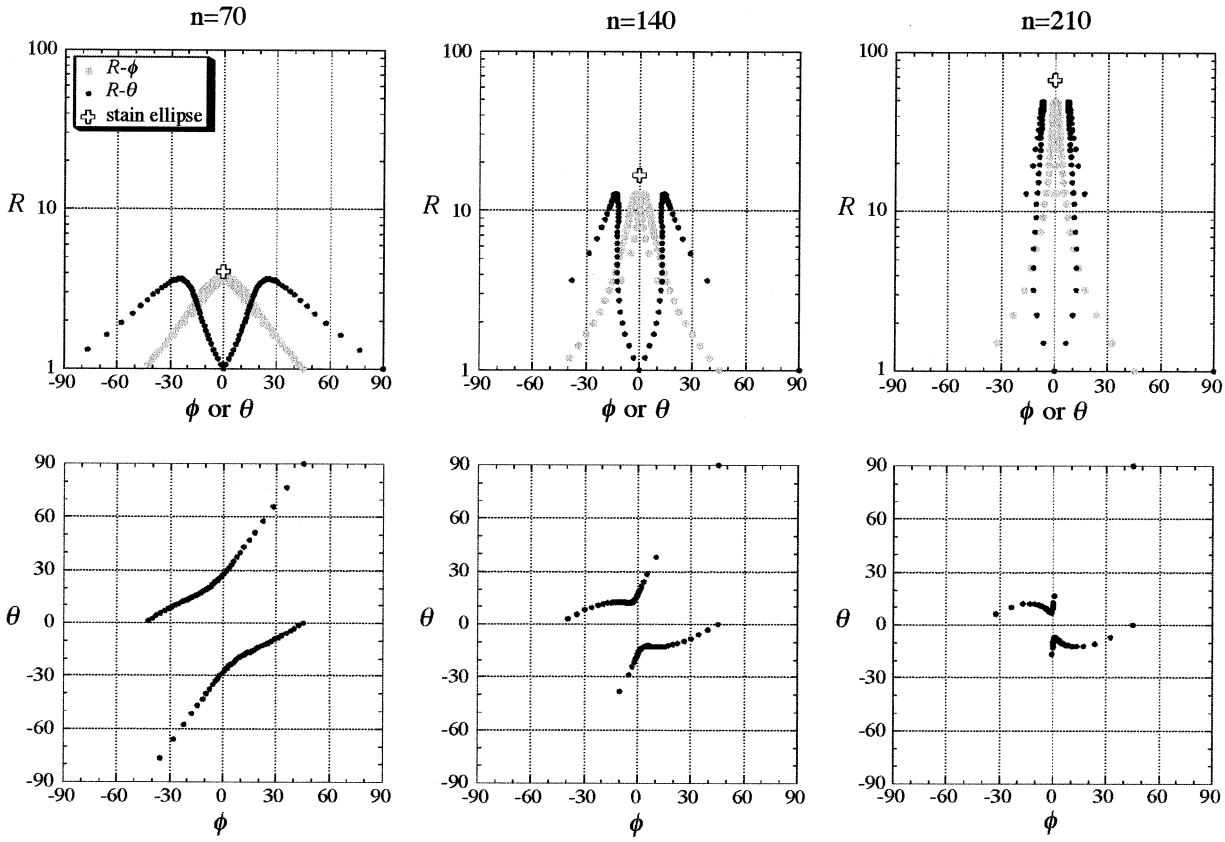

Fig. 10. Progressive development of lattice- and shape-preferred orientation of grains in a matrix deforming by progressive pure shear ($\Delta e = 0.01$, $\Delta\gamma = 0$).

However, for example, the grain with $\theta_0 = 50$ is transferred from one group to another as in the case of progressive simple shear.

4. A natural example

4.1. Analyzed sample and measurement

The Horoman peridotite complex (Niida, 1974, 1975, 1984; Obata and Nagahara, 1987; Takahashi, 1991, 1992; Takazawa et al., 1992, 1996, 1999, 2000; Ozawa and Takahashi, 1995) in the Hidaka metamorphic belt (Komatsu et al., 1989; Osanai et al., 1992), Hokkaido, Japan, is an Alpine-type peridotite massif, and is divided into five structural units on the basis of deformation microstructure (Fig. 14; Sawaguchi, 1999; Sawaguchi et al., 2001). The analyzed sample was collected from the internal shear zone where peridotites are mylonitized. This sample is harzburgite composed of olivine + orthopyroxene + spinel ± clinopyroxene. Olivine grains are completely recrystallized into a polygonal fine-grained (≈ 230 μm) matrix showing a

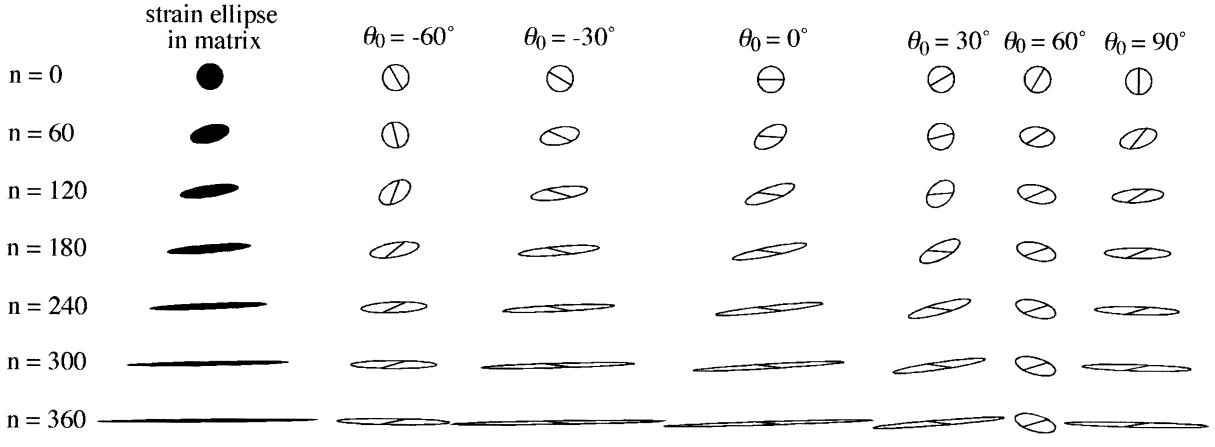

Fig. 11. Progressive deformation of grains with variable θ_0 in a matrix deforming by progressive general shear ($\Delta e = 0.005$, $\Delta\gamma = 0.01$).

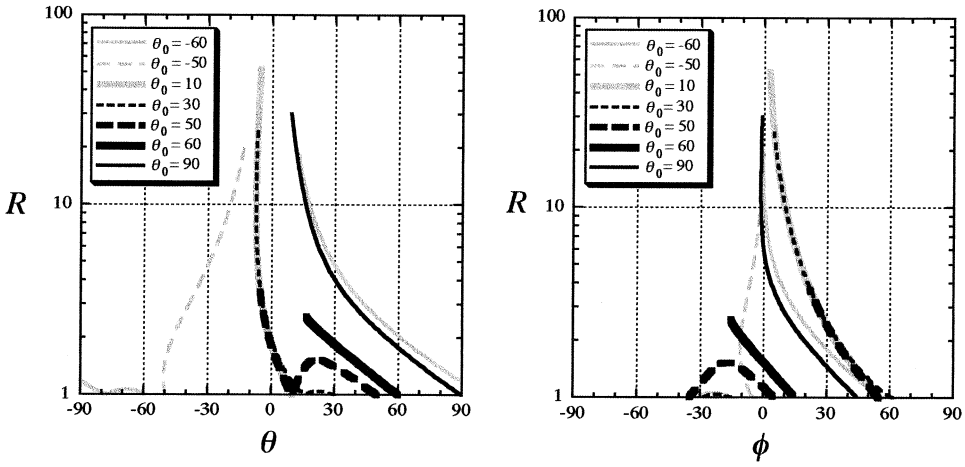

Fig. 12. Progressive change in R, θ and ϕ of grains with variable θ_0 in a matrix deforming by progressive general shear ($\Delta e = 0.005$, $\Delta\gamma = 0.01$) to $n = 360$.

strong lattice preferred orientation (Fig. 15a). The orientation of the olivine [100] point maximum is slightly oblique to the lineation. Orthopyroxene porphyroclasts are elongated to a variable extent defining structural elements such as foliation and lineation (Fig. 16). Grain size of orthopyroxene porphyroclasts ranges from 3 to 30 mm in long axis. They show wavy extinction, and exsolution lamellae of clinopyroxene along (100) are weakly curved over 10°. Some grains contain sub-grain boundaries or kink band boundaries normal to (100) exsolution lamellae. For extremely elongated orthopyroxene grains (aspect ratio $R > 10$), no recrystallization can be observed. In contrast, several grains with $R < 10$ show evidence of recrystallization along grain boundaries, that is fine-grained aggregates composed of orthopyroxene and olivine extending parallel to the lineation from the grains.

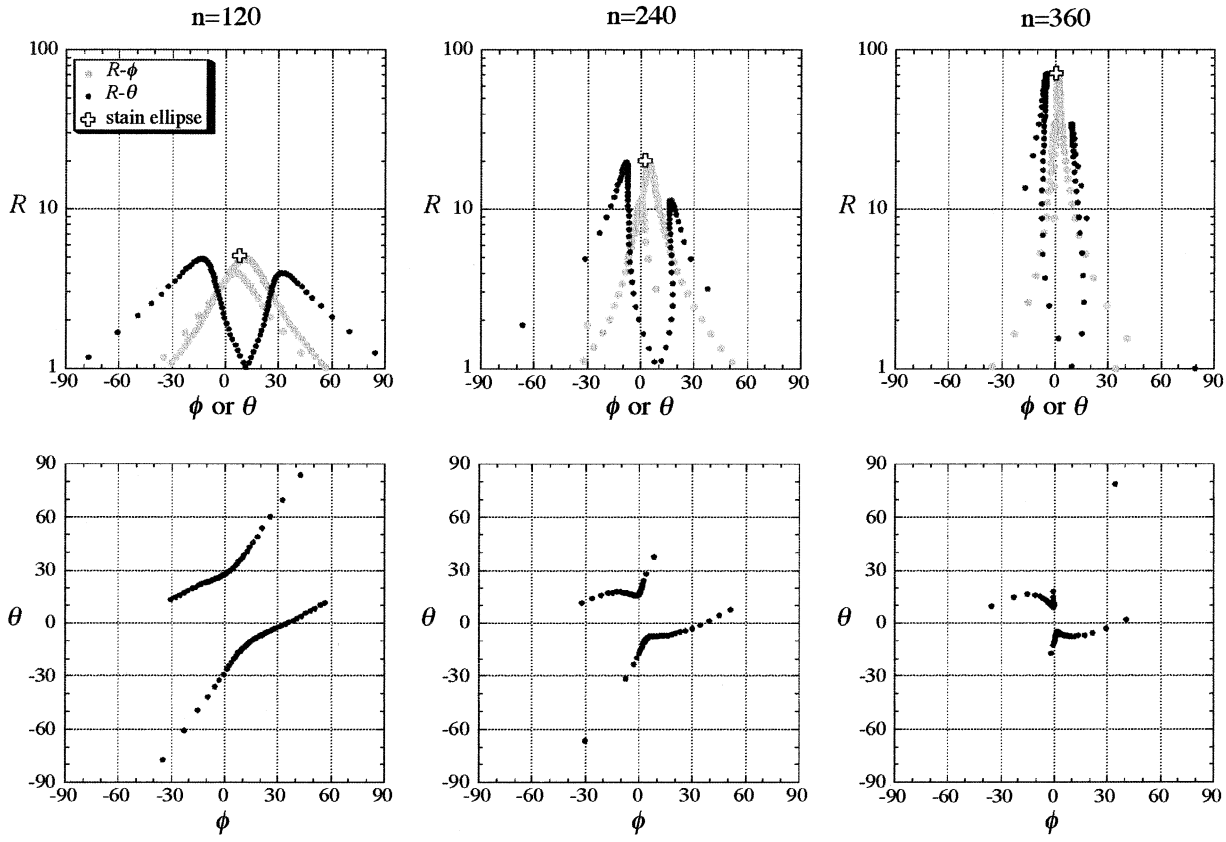

Fig. 13. Progressive development of lattice- and shape-preferred orientation of grains in a matrix deforming by progressive general shear ($\Delta e = 0.005$, $\Delta\gamma = 0.01$).

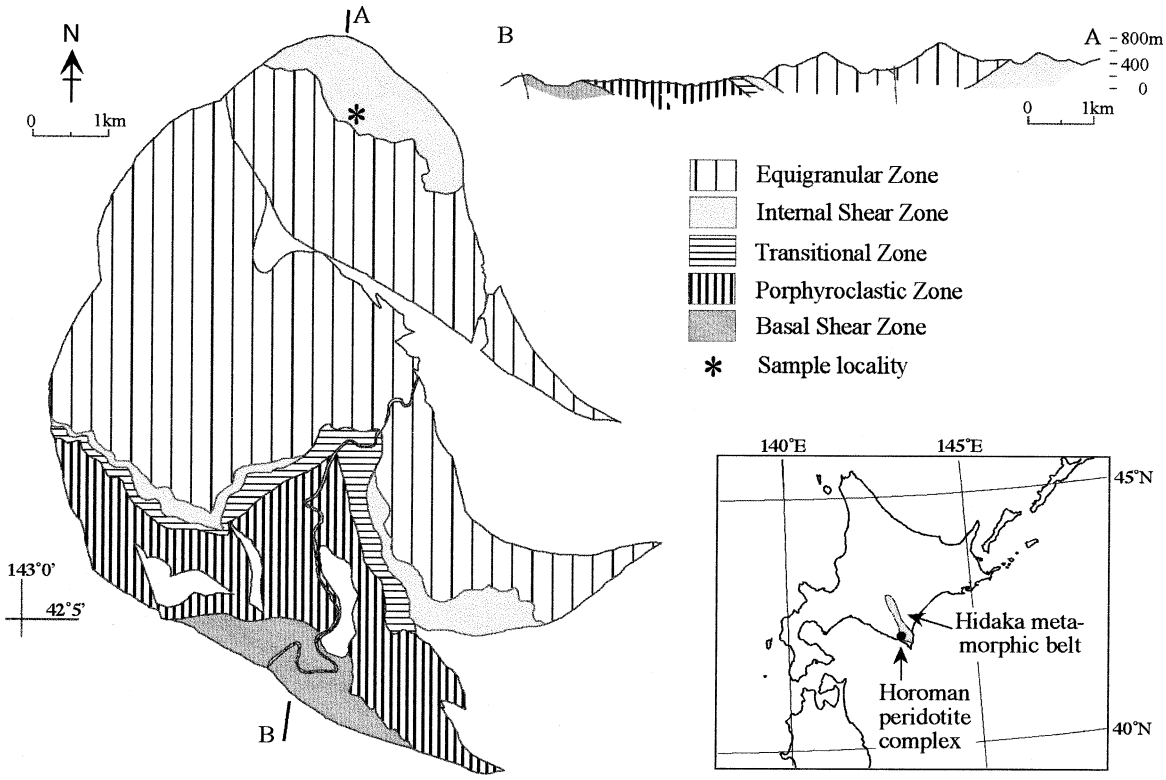

Fig. 14. Structural zones in the Horoman peridotite complex divided on the basis of olivine deformation microstructures (simplified from Sawaguchi et al., 2001). The insert shows the distribution of the Hidaka metamorphic belt and the Horoman peridotite complex.

Measurement of shape- and lattice-preferred orientation of orthopyroxene porphyroclasts has been carried out for thin sections cut parallel to the lineation and normal to the foliation (referred to as *XZ* plane hereafter). Orientations of crystallographic axes of 102 porphyroclasts from 12 *XZ* thin sections are measured with a petrographic microscope equipped with a U-stage. Their [100] and [001] orientations are sub-parallel to, but slightly oblique to, the foliation-normal and lineation, respectively. These distributions of lattice orientation for grains with the larger aspect ratio show the higher degree of concentration (Fig. 15b). In order to compare the natural results with those of the two-dimensional simulation, 19 orthopyroxene porphyroclasts whose [010] axes plunge over 80° with respect to thin section were selected. For these grains, the slip directions and the slip-plane normals of the (100)[001] slip system, that is [001] and [100], respectively, are oriented approximately within the *XZ* plane. This selection excludes almost circular grains ($R < 2$). Aspect ratio (R), long-axis orientation (ϕ') and orientation of the glide-plane trace (θ') were measured for these 19 grains under a microscope. Note that ϕ' and θ' are measured from the lineation. Because many porphyroclasts show lattice curvature expressed by wavy extinction or kink bands, we measured the range of glide-plane orientation (θ') for each orthopyroxene porphyroclast.

We cannot know the shape of grains before deformation, because almost all peridotites in the complex deform to a variable extent. However, we can estimate it to be nearly circular because the ratio of grain width normal to (100) to that parallel to (100) ranges from 0.7 to 1.5 in *XZ* section (w_b/w_a in Fig. 16b).

4.2. Results of measurements and comparison with simulations

Fig. 17a shows the R–θ', R–ϕ' and θ'–ϕ' relations of the 19 grains. Two groups can be distinguished from the θ'–ϕ' plot. While four grains plot in an area of $\theta' > \phi'$, others plot in an area of $\theta' < \phi'$. Grains with $\theta' < \phi'$ show relatively high R and their θ' ranges from -26 to 10°. Grains with $\theta' > \phi'$ show relatively low R and their θ' ranges from 9 to 36°. Maximum Rs of both groups are 23.9 and 5.6, respectively. ϕ'-distribution is concentrated around the lineation and ranges from -7 to 17°. There is no clear difference in the ranges of ϕ' between the two groups. The observed features are consistent with the simulation results. In particular, the asymmetrical R–θ' distribution in this natural example is more comparable with that of the simple shear simulation than with those of the pure and general shear simulations. Asymmetrical lattice preferred orientation of olivine (Fig. 15a) also supports non-coaxial deformation. We compare the result of the natural example with that of a progressive simple shear simulation after 220 deformation increments (Fig. 17b). In Fig. 17b, θ' and ϕ' are the glide-plane orientation and long-axis orientation measured from the elongation axis of matrix

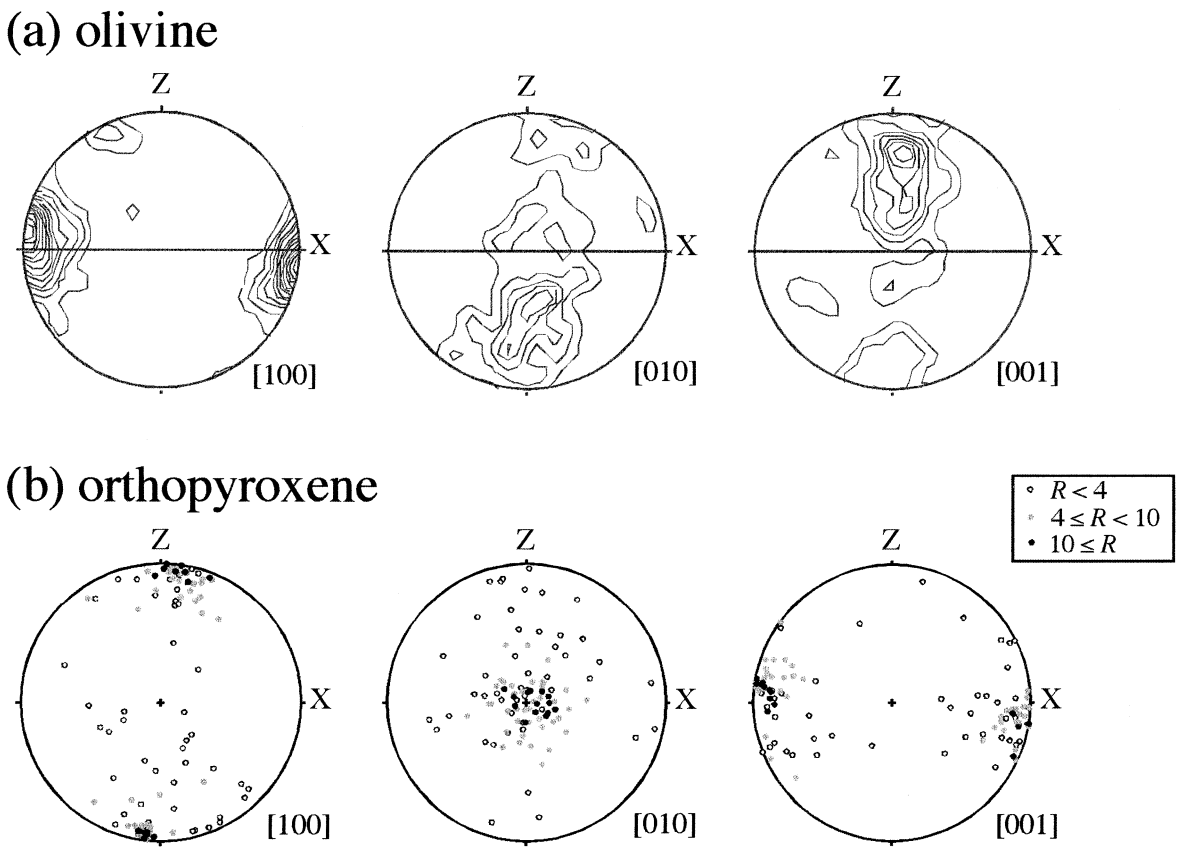

Fig. 15. Lattice preferred orientation of olivine (a) and orthopyroxene (b) measured on an *XZ* section. *X* and *Z* are the lineation and the normal to foliation, respectively. Contour interval in (a) is 1%. The symbols in (b) indicate aspect ratio (*R*) of orthopyroxene grains in *XZ* section. 100 (a) and 102 (b) grains are measured.

deformation, respectively. The degree of asymmetry in the natural $R-\theta'$ distribution is larger than the simulated one, because the maximum *R*s of grains in two simulated groups are 25.0 and 8.2, respectively. The results of 2-dimensional simulation can only be applied to plane-strain deformation. The lattice-preferred orientation of orthopyroxene porphyroclasts with a girdle distribution of [100] and [001], can be expected to develop by a constrictional and flattening deformation, respectively. The lattice-preferred orientation of the present natural sample, which shows a point concentration of [100] and [001] (Fig. 14b), roughly indicates plane-strain deformation.

5. Discussion and summary

5.1. Variation in the simulated lattice- and shape-preferred orientations

The simulation results show that glide-plane orientations (θ) of elongated grains are separated into two groups during progressive matrix deformation ranging from simple to pure shear. The degree of asymmetry in the $R-\theta$ distribution increases with increasing degree of non-coaxiality of matrix deformation. This is clearly reflected in the difference in maximum *R* of the two groups. In matrix deformation of progressive simple shear, glide-plane orientations (θ) of grains of the large-*R* group are concentrated around the shear plane of matrix deformation. On the other hand, the long-axis orientations (ϕ) of grains are concentrated around the elongation axis of matrix deformation. In addition, the shape (*R*) and the long-axis orientation (ϕ) of the grains with maximum *R* are nearly the same as those of the finite strain ellipse for matrix deformation. Therefore it is possible to estimate the geometry of the finite strain ellipse and the degree of non-coaxiality in natural peridotite based on lattice- and shape-preferred orientation of orthopyroxene porphyroclasts. Reuber et al. (1982) estimates qualitatively the deformation geometry ('relative importance' of simple and pure shear) of the Beni Bousera peridotites in Morocco from the relative abundance of orthopyroxene porphyroclasts deforming with opposite shear sense ($\phi < \theta$ or $\phi > \theta$ in the present notation). The present method using $R-\theta-\phi$ relation may provide a quantitative estimate on the degree of non-coaxiality.

The $R-\theta-\phi$ relation of the natural example is consistent with the simulation results and therefore shows the validity of the present model. We expect that further analysis of natural examples with a different $R-\theta-\phi$ relation will ensure the applicability of the present model.

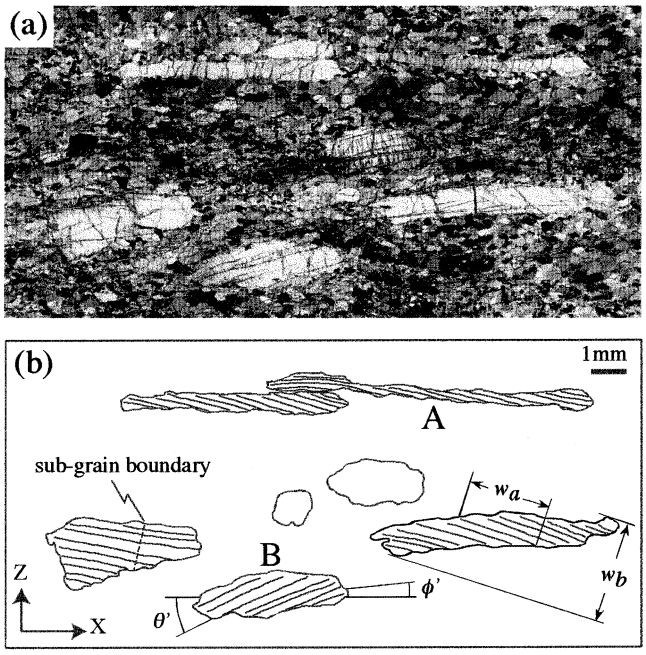

Fig. 16. (a) Photomicrograph of orthopyroxene porphyroclasts in the peridotite mylonite. Polarizers are not crossed entirely. (b) Schematic drawing showing the outline of orthopyroxene grains and the trace of slip plane (100). *X* and *Z* are lineation and normal to foliation, respectively. Results of measurements for two grains are also shown. Other grains are excluded from the analysis due to unsuitable lattice orientations. w_a and w_b indicate the grain width parallel and normal to the (100) trace, respectively.

5.2. Comparison with previous models of texture development

Wenk et al. (1991) simulated the development of lattice-preferred orientation of 'peridotite' (two-phase aggregates of 70% olivine–30% orthopyroxene). Their model, using the viscoplastic self-consistent theory, allows heterogeneous deformation depending on crystallographic orientation and assumes an actually single slip system (100)[001] of orthopyroxene. Their results for pure and simple shear deformation show that the [001] orientation of orthopyroxene becomes concentrated around the long axis of the strain ellipsoid. This is inconsistent with the present simulation results, probably because they only consider the plastic spin due to slip and not the rotation due to grain shape.

On the other hand, Etchecopar (1977) has simulated the development of lattice-preferred orientation of polycrystalline aggregates with a single slip system, using a purely geometrical model. His results show that glide-plane orientations become separated into two orientations during progressive pure shear and simple shear and that these two orientations are oblique to the long axis of the strain ellipse. In addition, for simple shear deformation one of them is sub-parallel to the shear plane. Zhang et al. (1994) have simulated the development of lattice-preferred orientation of polycrystalline aggregates with a single slip system. Their model, using the finite difference method, allows both inter- and intra-grain inhomogeneous deformation while ensuring strain compatibility and overall stress equilibrium. For both pure and simple shear deformation, their results show the same glide-plane orientations as those in Etchecopar (1977). In addition, their results show that long-axis orientations of deformed grains are concentrated parallel to the long axis of the strain ellipse. These results of Etchecopar (1977) and Zhang et al. (1994) are consistent with the present results.

Some natural mylonitic rocks show orthopyroxene [001] orientation oblique to the lineation (e.g. Mercier, 1985; Dornbusch et al., 1994). These lattice-preferred orientations are similar to the present natural example (Fig. 14b) and are consistent with the present simulation results.

5.3. Rheological contrast between grains and the matrix

The present purely geometrical simulation model makes the following assumptions. Under a given matrix deformation, orthopyroxene grains deform and rotate so as to minimize the difference in displacement between the matrix and the grains. This means that orthopyroxene grains are sufficiently 'soft' relative to the matrix (i.e. fine-grained olivine aggregates). If orthopyroxene grains are significantly 'harder' than the matrix, the shear deformation of grains (β) are considered to be smaller than those in the present simulation results. The increase in rigid body rotation of the grains (ω) possibly compensates for such a decreased amount of deformation so as to reduce the difference in

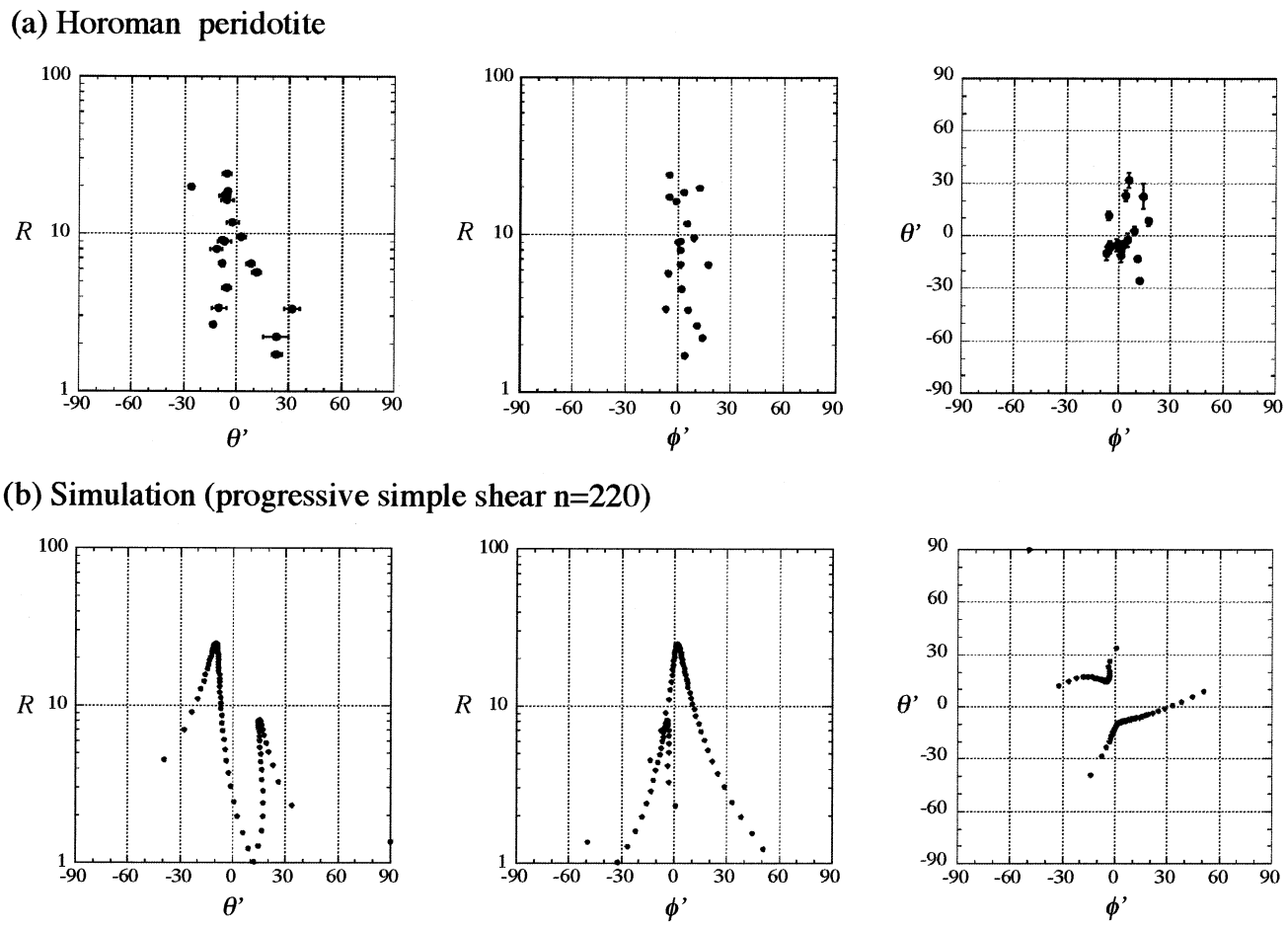

Fig. 17. Comparison of lattice- and shape-preferred orientation of orthopyroxene porphyroclasts between a natural sample (a) and a simulation (b). R; aspect ratio, θ'; orientation of the glide plane, ϕ'; orientation of the long axis. θ' and ϕ' in (a) are measured from the lineation, and those in (b) are orientations with respect to elongation axis of matrix deformation. 'Error bars' in (a) indicate ranges of θ' for each grain.

displacement between the matrix and the grains. Therefore, in the case of 'harder' grains, the ratio of rotation to deformation (ω/β) for each grain may be larger than that in the present simulation results. This change in 'partitioning' between deformation and rotation must alter the $R-\theta-\phi$ relations. Consider, for example, the grains forming the second group in matrix deforming by progressive simple shear (Figs. 5 and 6). We can expect the following two effects of increasing ratio of rotation to deformation for these grains. Firstly, their Rs should be lower than the result of the present simulation. Secondly, there should be more rapid transfer of these grains to the first group. Therefore, the difference in the degree of asymmetry in $R-\theta$ distribution between the natural and simulated examples (Fig. 16) may be attributed to this rheological contrast.

Mackwell (1991) has performed high-temperature deformation experiments at atmospheric pressure on single-crystal enstatite under well-controlled chemical, thermal and mechanical conditions. His results show that the strength of (100)[001] slip systems in enstatite is softer than some olivine slip systems at high temperature and harder than olivine at lower temperatures. Therefore, it seems to be possible in natural environments that orthopyroxene porphyroclasts have strength nearly equal to or slightly larger than the fine-grained olivine matrix.

5.4. Recrystallization and fracturing of orthopyroxene grains

In the present simulation, some grains show very small rotation and deformation rates. Examples are the grains with $-60° \leq \theta_0 \leq -30°$ during the deformation stage $n = 180$–360 in a matrix deforming by progressive simple shear and the grain with $\theta_0 = 60°$ during the deformation stage $n = 120$~360 in a matrix deforming by progressive general shear (Figs. 5, 6, 11 and 12). Etchecopar (1977) and Etchecopar and Vasseur (1987) consider that these 'locked' grains disappear through several 'unlocking' processes, including fracturing, heterogeneous deformation and recrystallization. The fracturing of a 'locked' grain normal to its elongation gives smaller and more isodiametric grains, which enables further rotation. The heterogeneous deformation such as flexuring and twisting allow a progressive unlocking of part of the grain. The recrystallization of a

deformed grain creates new grains with different shape and crystallographic orientation.

Orthopyroxene grains in the present natural sample shows no clear evidence of fracturing and heterogeneous deformation except for wavy extinction and weak curvature of (100) lamellae. In addition, orthopyroxene is deformed plastically, predominantly without recrystallization, although several grains with $R < 10$ show some evidence of recrystallization along the grain boundary, as mentioned before. Therefore, these processes do not seem to affect the $R-\theta-\phi$ relation to a large extent in the present natural sample.

Acknowledgements

We thank T. Takeshita, K. Kanagawa and H. Takagi for valuable discussion and improvements of early version of the manuscript. We are also grateful to M. Drury and an anonymous referee for their constructive reviews.

References

Darot, M., Boudier, F., 1975. Mineral lineations in deformed peridotites: kinematic meaning. Petrologie 1, 225–236.

Dornbusch, H.-J., Weber, K., Skrotzki, W., 1994. Development of microstructure and texture in high-temperature mylonites from the Ivrea Zone. In: Bung, H.J., Siegesmund, S., Skrotzki, W., Weber, K. (Eds.). Textures of Geological Materials. DGM Informationsgesellschaft, Oberursel, pp. 187–201.

Etchecopar, A., 1977. A plane kinematic model of progressive deformation in a polycrystalline aggregate. Tectonophysics 39, 121–139.

Etchecopar, A., Malavieille, J., 1987. Computer models of pressure shadows: a method for strain measurement and shear-sense determination. Journal of Structural Geology 9, 667–677.

Etchecopar, A., Vasseur, G., 1987. A 3-D kinematic model of fabric development in polycrystalline aggregates: comparisons with experimental and natural examples. Journal of Structural Geology 9, 705–717.

Hanmer, S., 2000. Matrix mosaics, brittle deformation, and elongate porphyroclasts: granulite facies microstructures in the Striding–Athabasca mylonite zone, western Canada. Journal of Structural Geology 22, 947–967.

Ishii, K., 1995. Estimation of non-coaxiality from crinoid-type pressure fringes: comparison between natural and simulated examples. Journal of Structural Geology 17, 1267–1278.

Jessel, M.W., 1988a. Simulation of fabric development in recrystallizing aggregates. I. Description of the model. Journal of Structural Geology 10, 771–778.

Jessel, M.W., 1988b. Simulation of fabric development in recrystallizing aggregates. II. Example model runs. Journal of Structural Geology 10, 779–793.

Jessel, M.W., Lister, G.S., 1990. A simulation of the temperature dependence of quartz fabric. In: Knipe, R.J., Rutter, E.H. (Eds.). Deformation Mechanisms, Rheology and Tectonics. Special Publication of the Geological Society London, 54, pp. 353–362.

Komatsu, M., Oasanai, Y., Toyoshima, T., Miyashita, S., 1989. Evolution of the Hidaka metamorphic belt, northern Japan. Journal of the Geological Society of London, Special Publication 43, 487–493.

Lister, G.S., Paterson, M.S., 1979. The simulation of fabric development during plastic deformation and its application to quartzite: fabric transitions. Journal of Structural Geology 1, 99–115.

Lister, G.S., Hobbs, B.E., 1980. The simulation of fabric development during plastic deformation and its application to quartzite: the influence of deformation history. Journal of Structural Geology 2, 355–370.

Lister, G.S., Paterson, M.S., Hobbs, B.E., 1978. The simulation of fabric development during plastic deformation and its application to quartzite: the model. Tectonophysics 45, 107–158.

Mackwell, S.J., 1991. High-temperature rheology of enstatite: Implications for creep in the mantle. Geophysical Research Letters 18, 2027–2030.

Mercier, J.-C.C., 1985. Olivine and pyroxenes. In: Wenk, H.-R. (Ed.). Preferred Orientation in Deformed Metals and Rocks: An Introduction to Modern Texture Analysis. Academic Press, Orlando, pp. 407–430.

Molinari, A., Canova, G.R., Ahzi, S., 1987. A self-consistent approach of the large deformation polycrystal viscoplasticity. Acta Metallurgica 35, 2983–2994.

Niida, K., 1974. Structure of the Horoman ultramafic mass of the Hidaka metamorphic belt in Hokkaido, Japan. The Journal of the Geological Society of Japan 80, 31–44.

Niida, K., 1975. Texture of olivine fabrics and the Horoman ultramafic rocks, Japan. Journal of Mineralogy, Petrology and Economic Geology 70, 265–285.

Niida, K., 1984. Petrology of the Horoman ultramafic rocks. Journal of the Faculty of Science, Hokkaido University, Series IV 21, 61–81.

Obata, M., Nagahara, N., 1987. Layering of alpine-type peridotite and the segregation of partial melt in the upper mantle. Journal of Geophysical Research 92, 3467–3474.

Osanai, Y., Owada, M., Kawasaki, T., 1992. Tertiary deep crustal ultrametamorphism in the Hidaka metamorphic belt, northern Japan. Journal of Metamorphic Geology 10, 401–414.

Ozawa, K., Takahashi, N., 1995. P–T history of a mantle diapir: the Horoman peridotite complex, Hokkaido, northern Japan. Contributions to Mineralogy and Petrology 120, 223–248.

Reuber, I., Michard, A., Chalouan, A., Juteau, T., Jermoumi, B., 1982. Structure and emplacement of the Alpine-type peridotites from Beni Bousera, Rif, Morocco: a polyphase tectonic interpretation. Tectonophysics 82, 231–251.

Sawaguchi, T., 1999. Deformation history of the Horoman peridotite complex, Hokkaido, Japan. Ofioliti 24, 163.

Sawaguchi, T., Takagi, H., 1997. Inverted ductile shear movement of the Horoman peridotite complex in the Hidaka metamorphic belt, Hokkaido, Japan. The Memoirs of the Geological Society of Japan 47, 193–208.

Sawaguchi, T., Goto, K., Takagi, H., 2001. Elongated orthopyroxene porphyroclast as a shear sense indicator and kinematic history of the Horoman Peridotite Complex, Hokkaido, Japan. The Journal of the Geological Society of Japan 107, 165–178.

Suhr, G., 1993. Evaluation of upper mantle microstructures in the Table Mountain massif (Bay of Islands ophiolite). Journal of Structural Geology 15, 1273–1292.

Takahashi, N., 1991. Origin of three Peridotite suites from Horoman peridotite complex, Hokkaido Japan; melt segregation and solidification process in the upper mantle. Journal of Mineralogy, Petrology and Economic Geology 86, 199–215.

Takahashi, N., 1992. Evidence for melt segregation toward features in the Horoman mantle peridotite complex. Nature 359, 52–55.

Takazawa, E., Frey, F.A., Obata, M., Bodinier, J.L., 1992. Geochemical evidence for melt migration and reaction in the upper mantle. Nature 359, 55–58.

Takazawa, E., Frey, F.A., Shimizu, N., Obata, M., 1996. Evolution of the Horoman peridotite: implications from pyroxene compositions. Chemical Geology 134, 3–26.

Takazawa, E., Frey, F.A., Shimizu, N., Saal, A., Obata, M., 1999. Polybaric petrogenesis of mafic layers in the Horoman Peridotite Complex, Japan. Journal of Petrology 40, 1827–1851.

Takazawa, E., Frey, F.A., Shimizu, N., Obata, M., 2000. Whole rock compositional variations in an upper mantle peridotite (Horoman, Hokkaido, Japan): are they consistent with a partial melting process?. Geochimica et Cosmochimica Acta 64, 695–716.

Takeshita, T., Wenk, H.-R., Molinari, A., Canova, G.R., 1990. Simulation

of dislocation-assisted plastic deformation in olivine polycrystals. In: Barber, D.J., Meredith, P.G. (Eds.). Deformation Mechanisms in Minerals, Ceramics and Rocks. Unwin Hyman Ltd, London, pp. 365–376.

Taylor, G.I., 1938. Plastic strain in metals. Journal of the Institute of Metals 62, 307–324.

Toyoshima, T., 1998. Gabbro mylonite developed along a crustal-scale décollement. In: Snoke, A.W., Tullis, J., Todd, V.R. (Eds.). Fault-related Rocks: A Photographic Atlas. Princeton University Press, Princeton, pp. 426–427.

Tubía, J.M., 1994. The Ronda peridotites (Los Reales nappe): an example of the relationship between lithospheric thickening by oblique tectonics and late extensional deformation within the Betic Cordillera (Spain). Tectonophysics 238, 381–398.

Wenk, H.-R., Tomé, C.M., 1999. Modeling dynamic recrystallization of olivine aggregates deformed in simple shear. Journal of Geophysical Research 104, 25513–25527.

Wenk, H.-R., Canova, G., Molinari, A., Kocks, U.F., 1989. Viscoplastic modeling of texture development in quartzite. Journal of Geophysical Research 94, 17895–17906.

Wenk, H.-R., Bennett, K., Canova, G., Molinari, A., 1991. Modeling plastic deformation of peridotite with the self-consistent theory. Journal of Geophysical Research 96, 8337–8349.

Zhang, Y., Wilson, C.J.L., 1997. Lattice rotation in polycrystalline aggregates and single crystals with one slip system: a numerical and experimental approach. Journal of Structural Geology 19, 875–885.

Zhang, Y., Hobbs, B.E., Ord, A., 1994. A numerical simulation of fabric development in polycrystalline aggregates with one slip system. Journal of Structural Geology 16, 1297–1313.